Journal of Neurology (2019) 266:844–859
https://doi.org/10.1007/s00415-019-09204-4

ORIGINAL COMMUNICATION

Transient seizure onset network for localization of epileptogenic zone: effective connectivity and graph theory-based analyses of ECoG data in temporal lobe epilepsy

Ye Ren[1,2] · Fengyu Cong[2,3] · Tapani Ristaniemi[2] · Yuping Wang[4,5,6] · Xiaoli Li[7] · Ruihua Zhang[1]

Received: 24 August 2018 / Revised: 20 December 2018 / Accepted: 18 January 2019 / Published online: 25 January 2019

Abstract

Objective Abnormal and dynamic epileptogenic networks cause difficulties for clinical epileptologists in the localization of the seizure onset zone (SOZ) and the epileptogenic zone (EZ) in preoperative assessments of patients with refractory epilepsy. The aim of this study is to investigate the characteristics of time-varying effective connectivity networks in various non-seizure and seizure periods, and to propose a quantitative approach for accurate localization of SOZ and EZ.

Methods We used electrocorticogram recordings in the temporal lobe and hippocampus from seven patients with temporal lobe epilepsy to characterize the effective connectivity dynamics at a high temporal resolution using the full-frequency adaptive directed transfer function (ffADTF) measure and five graph metrics, i.e., the out-degree (OD), closeness centrality (CC), betweenness centrality (BC), clustering coefficient (C), and local efficiency (LE). The ffADTF effective connectivity network was calculated and described in five frequency bands (δ, θ, α, β, and γ) and five seizure periods (pre-seizure, early seizure, mid-seizure, late seizure, and post-seizure). The cortical areas with high values of graph metrics in the transient seizure onset network were compared with the SOZ and EZ identified by clinical epileptologists and the results of epilepsy resection surgeries.

Results Origination and propagation of epileptic activity were observed in the high time resolution ffADTF effective connectivity network throughout the entire seizure period. The seizure-specific transient seizure onset ffADTF network that emerged at seizure onset time remained for approximately 20–50 ms with strong connections generated from both SOZ and EZ. The values of graph metrics in the SOZ and EZ were significantly larger than that in the other cortical areas. More cortical areas with the highest mean of graph metrics were the same as the clinically determined SOZ in the low-frequency δ and θ bands and in Engel Class I patients than in higher frequency α, β, and γ bands and in Engel Class II and III patients. The OD and C were more likely to localize the SOZ and EZ than CC, BC, and LE in the transient seizure onset network.

Conclusion The high temporal resolution ffADTF effective connectivity analysis combined with the graph theoretical analysis helps us to understand how epileptic activity is generated and propagated during the seizure period. The newly discovered seizure-specific transient seizure onset network could be an important biomarker and a promising tool for more precise localization of the SOZ and EZ in preoperative evaluations.

Keywords Adaptive directed transfer function · Graph metric · Brain connectivity · Seizure onset zone · Epileptogenic zone

Introduction

Temporal lobe epilepsy (TLE) is the most common form of medically intractable epilepsy, which is increasingly seen as a disorder of the epileptogenic networks that lead to connectivity disturbances [3, 5, 10]. Abnormal activity in the epileptic connectivity network makes it difficult for epileptologists to locate the seizure onset zone (SOZ), epileptogenic zone (EZ), and resective region, which may lead to the failure of resection surgery or various degrees of postoperative

✉ Xiaoli Li
xiaoli@bnu.edu.cn

✉ Ruihua Zhang
ruihua.zhang@ccmu.edu.cn

Extended author information available on the last page of the article

seizures in these drug-resistant epilepsy patients. Accurate localization of SOZ and EZ during preoperative assessment and precise resection of these cortical areas during epilepsy surgery are vital for patients with TLE. The aim of this paper is to investigate the characteristics of time-varying effective connectivity networks in patients with TLE, and to propose a quantitative approach for more accurate localization of SOZ and EZ using the effective connectivity and graph theoretical analyses.

Effective connectivity [8] refers to causal interactions among the neural elements [36], thus describing the directed connections in the brain network. Granger causality (GC) is one of the prototypical data-driven effective connectivity techniques [19]. Directed transfer function (DTF), a GC-based effective connectivity measure, was proposed by Kaminski and Blinowska [11] to reveal the direction of the information flow between multiple signals in the frequency domain of the brain. DTF has been used to assess interictal and preictal activity to indicate an upcoming seizure [37], and to assess ictal activity to localize the EZ in medically intractable epilepsy patients [33, 35]. However, DTF assumes the stationarity of neural signals and the time invariance of network connectivity in a short time window. That is, the connectivity pattern obtained by DTF is unchanged over the analyzed time period.

Wilke et al. [31] proposed an adaptive DTF (ADTF) measure using an adaptive multivariate autoregressive (AMVAR) model for detecting the dynamic changes of the information interactions and used ADTF to study the time-variant connectivity of seizures and interictal spikes [32]. Having high temporal resolution, this effective connectivity measure is able to address non-stationary signals, thus capturing the temporal dynamics of network connectivity at specified frequencies, which the DTF measure cannot. The ADTF has been used to reveal dynamic brain network patterns and to detect EZ during the interictal electroencephalography (EEG) [38]. In addition, the full-frequency ADTF (ffADTF) that measures the effective connectivity in a specific frequency band has been used to describe the propagation patterns of electrocorticogram (ECoG) recordings of seizure onsets across brain areas and proved that it outperforms the other normalizations of ADTF in locating the EZ [26].

Graph theory allows a network-based representation of TLE brain networks, which has the potential to illuminate the characteristics of brain topology [1]. Different electrophysiologic and neuroimaging modalities have used graph theory to identify EZ, predict seizures, and assess cognitive performance in TLE [10]. In terms of localization, graph theoretical measures, including out-degree (OD), betweenness centrality (BC), and graph index complexity, have shown the most potential [10]. It was found through simulation data and ictal or interictal patient data that the ADTF and normalizations of the ADTF measures combined with the OD resulted in correct SOZ and EZ localization [25, 27, 38]. In addition, ADTF combined with BC was applied to ictal and interictal ECoG, and was found to correlate with the resected cortical regions [34]. It was also used to assess interictal spikes on EEG recording, confirming that this combination was effective at detecting the focal regions and characterizing the dynamics of the spike propagation [23]. Closeness centrality (CC) has been used to predict an upcoming seizure [37] and describe the change of network topology at seizure onset [13]. ECoG studies have determined the increase in clustering coefficient (C) during the ictal compared to interictal phase [12, 16]. Local efficiency (LE) has been found to be correlated positively with the epilepsy duration in the resting-state fMRI data of TLE patients [29]. However, effective connectivity features of epileptic activity in different frequency bands during non-seizure and various seizure periods in the epileptic network have not been clearly elaborated in these previous studies. A few studies have compared the performance of different graph theoretical measures for localization of the SOZ and EZ in TLE.

In this study, we investigated the time-varying characteristics of effective connectivity network using the ffADTF measure and five graph metrics (OD, CC, BC, C, and LE) in 14 seizures of seven patients with TLE. The ffADTF effective connectivity network was compared in five frequency bands (δ, θ, α, β, and γ), five representative seizure periods (pre-seizure, early seizure, mid-seizure, late seizure, and post-seizure), as well as the SOZ and resected regions that were identified by the clinical epileptologists and the results of epilepsy surgery. The results showed that the high temporal resolution ffADTF could provide more information about the origination and propagation of seizures. More cortical areas with the highest mean of OD and C were the same as the clinically determined SOZ in the low-frequency δ and θ bands. The seizure-specific transient seizure onset network could lead to a more accurate localization of SOZ and EZ, helping us to understand the neuroelectrophysiological mechanism of epileptic seizures and improving the accuracy of preoperative evaluations of patients with refractory epilepsy.

Materials and methods

Data recording and preprocessing

We obtained multichannel ECoG data from subdural electrode strips implanted in seven patients with TLE before resective epilepsy surgery. All patients were provided with written informed consent. The clinical information regarding these patients is illustrated in Table 1. Surgical outcomes were classified according to Engel's

Table 1 Clinical information of the patients with temporal lobe epilepsy

Patient/sex/age (years)	Electrode strip placement/total number of electrode contacts	SOC	SOZ	Resected regions	Follow-up (months)/ surgical outcome (Engel Class)
A/F/24	LH (6×1), LTP (8×1), LTB (8×1) RH (6×1), RTP (8×1), RTB (8×1)/44	10	RH	RH, RTP, RTB	26/I
B/F/46	LTP (8×1), LTB (8×1) RTP (8×1), RTB (8×1)/32	1, 2	LTP	LTP, LTB	53/II
C/M/22	LH (8×1), LTB (8×1), LPTB (8×1) RH (8×1), RTB (8×1), RPTB (8×1)/48	3, 11	LH, LTB	LH, LTB	55/II
D/M/33	LH (6×1), LTP (6×1), LTB (8×1) RH (6×1), RTP (6×1), RTB (6×1)/38	1, 2, 3, 4	LH	LH, LTP, LTB	54/I
E/F/28	RH (4×1), RTP (8×2), RTB (6×1) RPTL (8×1), RFPL (8×2)/50	25, 26	RTP	RH, RTP, RTB	27/I
F/F/28	LTP (8×1), LTB (8×1), LTO (8×1) RTP (8×1), RTB (8×1), RTO (8×1)/48	5, 6, 7	RTP	RTP, RTB	34/III
G/M/21	LTP (8×1), LTB (8×1), LTO (8×1) RTP (8×1), RTB (8×1), RTO (8×1)/48	6, 7, 8	RTP	RTP, RTB	29/III

F female, *M* male, *L* left, *R* right, *H* hippocampus, *TL* temporal lobe, *TP* temporal pole, *TB* temporal base, *PTL* posterior temporal lobe, *PTB* posterior temporal base, *FPL* frontal–parietal lobe, *TO* temporal–occipital, *SOC* seizure onset channel, *SOZ* seizure onset zone

classification [4] into Class I: Free of disabling seizures, Class II: Rare disabling seizures ("almost seizure-free"), Class III: Worthwhile improvement, and Class IV: No worthwhile improvement. Cortical electrode strips (2.5-mm-diameter platinum electrodes positioned 10-mm apart centre-to-centre) were placed on the temporal lobe and other cortical areas. Depth electrodes (1.2-mm-diameter platinum electrodes positioned 10-mm apart centre-to-centre) were implanted in the hippocampus.

ECoG was continuously recorded day and night for the preoperative assessments of all patients using a video-EEG monitoring system (PN-NET, Beijing Yunshen Technology, China). Electrode contacts, which were located far from the epileptogenic lesion, were used as the reference electrode contact. The sampling frequency of the ECoG data was 2048 Hz. The ECoG data of 14 seizures from seven patients, which included complete spontaneous epileptic seizures, were selected for analysis. An ECoG data segment was cut from approximately 1 min before seizure onset to approximately 1 min after seizure termination. These data were first exported as European Data Format Plus (EDF+) files and then imported into EEGLAB to convert the file format to MAT. Then, the files were down-sampled to 256 Hz and filtered with a 0.2-Hz high-pass filter to remove baseline interference. Standardized z-scores were also used to normalize the variance of the ECoG data in each channel. Power frequency noise (50 Hz) and harmonic noises were removed by a notch filter. Large-amplitude artifacts were removed, and bad channels were rejected by visual inspection.

Effective connectivity analysis

The ADTF measure was adopted to quantify the causal connection feature among different cortical areas. The ADTF developed by Wilke et al. [32] is based on the concept of GC [9], which can capture the temporal dynamics of the models. According to GC, if a signal x_1 can be predicted by the past information from a signal x_2 better than the past information from its own signal, then the signal x_2 can be considered causal to the signal x_1 [19]. A common way to model GC is using the autoregressive modelling technique. The pre-processed ECoG data epoch is modelled using the AMVAR model and is represented as a combination of its own past as follows:

$$\boldsymbol{X}(t) = \sum_{m=1}^{p} \boldsymbol{A}_m(t)\boldsymbol{X}(t-m) + \boldsymbol{E}(t), \tag{1}$$

where $\boldsymbol{X}(t)$ is the signal matrix, $\boldsymbol{A}_m(t)$ is the $K \times K$ model coefficient matrix for delay m, K is the number of signal channels, p is the model order, and $\boldsymbol{E}(t)$ is the uncorrelated white noise matrix. Equation (1) can be given by the following:

$$\begin{bmatrix} \boldsymbol{x}_1(t) \\ \vdots \\ \boldsymbol{x}_K(t) \end{bmatrix} = \sum_{m=1}^{p} \begin{bmatrix} \boldsymbol{a}_{m,11}(t) & \cdots & \boldsymbol{a}_{m,1K}(t) \\ \vdots & \ddots & \vdots \\ \boldsymbol{a}_{m,K1}(t) & \cdots & \boldsymbol{a}_{m,KK}(t) \end{bmatrix} \begin{bmatrix} \boldsymbol{x}_1(t-m) \\ \vdots \\ \boldsymbol{x}_K(t-m) \end{bmatrix} + \begin{bmatrix} \boldsymbol{e}_1(t) \\ \vdots \\ \boldsymbol{e}_K(t) \end{bmatrix}. \tag{2}$$

MATLAB module ARfit [14, 21] was used (http://climate-dynamics.org/software/#arfit) to estimate the parameters of the model.

A lower bound $p_{\min}$ and an upper bound $p_{\max}$ were first given on the model order. For the estimation of the parameters coefficient matrices of the model $\boldsymbol{A}_1, \boldsymbol{A}_2, \ldots, \boldsymbol{A}_p$ and $K \times K$ noise covariance matrix C_p of the zero-mean white noise $\boldsymbol{E}(t)$, the stepwise least-squares algorithm is implemented for the models of successive orders $p_{\min}, \ldots, p_{\max}$ in ARfit. The optimal model order p_{opt} was selected according to the Schwarz's Bayesian criterion (SBC) [22]. The SBC can be calculated as follows:

$$\mathrm{SBC}(p) = \ln\left|C_p\right| + \frac{\ln(N)pK^2}{N}, \tag{3}$$

where C_p is the covariance matrix of the noises, N is the number of time points. p_{opt} corresponds with the minimum of the SBC function. The parameters $\boldsymbol{A}_1, \boldsymbol{A}_2, \ldots, \boldsymbol{A}_{opt}$ were then computed for a model of the optimal order p_{opt}. $p_{\min} = 1$, $p_{\max} = 5$ were set in our study and the p_{opt} was estimated for each data epoch, which ranged from 1 to 2.

To investigate the causality between the signals in the spectral domain, the Fourier transform was applied to Eq. (1):

$$\boldsymbol{E}(f) = \boldsymbol{A}(f)\boldsymbol{X}(f), \tag{4}$$

where the coefficient matrix is as follows:

$$\boldsymbol{A}(f) = \boldsymbol{I} - \sum_{m=1}^{p} \boldsymbol{A}_m e^{-i2\pi fm}, \tag{5}$$

where $\boldsymbol{I}$ is the $K \times K$ identity matrix. $\boldsymbol{E}(f)$, $\boldsymbol{A}(f)$ and $\boldsymbol{X}(f)$ are the Fourier transformation of the noise, the coefficient matrix, and the signal matrix, respectively. Under the assumption that the matrix $\boldsymbol{A}(f)$ is nonsingular and, thus, invertible, Eq. (2) can be written as follows:

$$\boldsymbol{X}(f) = \boldsymbol{A}^{-1}(f)\boldsymbol{E}(f) = \boldsymbol{H}(f)\boldsymbol{E}(f), \tag{6}$$

where $\boldsymbol{H}(f)$ is the $K \times K$ transfer matrix, which is the inverse of the Fourier transform of the coefficient matrix $\boldsymbol{A}(f)$:

$$\boldsymbol{H}(f) = \boldsymbol{A}(f)^{-1}. \tag{7}$$

The element $H_{ij}(f)$ contains information about the causality from the signal x_j to signal x_i at frequency f.

The AMVAR model, i.e., time-variant multivariate autoregressive (TVAR) model allows us to obtain the time-varying model coefficients $\boldsymbol{A}(f,t)$ at each time point t, which was estimated by the standard Kalman algorithm [20, 26].

The time-variant effective connectivity measures ADTF and normalized ADTF (nADTF) at each time point were then defined as follows:

$$\mathrm{ADTF}_{ij}(f,t) = |\boldsymbol{H}_{ij}(f,t)|^2. \tag{8}$$

$$\mathrm{nADTF}_{ij}(f,t) = \frac{|\boldsymbol{H}_{ij}(f,t)|^2}{\sum_{k=1}^{K}|\boldsymbol{H}_{ik}(f,t)|^2}. \tag{9}$$

The ffADTF in the specific frequency band $[f_1, f_2]$ from signal x_j to signal x_i was defined as follows:

$$\mathrm{ffADTF}_{ij}(t) = \frac{\sum_{f=f_1}^{f_2}|\boldsymbol{H}_{ij}(f,t)|^2}{\sum_{k=1}^{K}\sum_{f=f_1}^{f_2}|\boldsymbol{H}_{ik}(f,t)|^2}. \tag{10}$$

ffADTF is a normalization of ADTF, which incorporates the frequency information of all the frequencies in the defined frequency band $[f_1, f_2]$ at each time point. The value of ffADTF is an interval [0, 1], which is used as edge weight and represents the connection strength in the network. The sum of the incoming information flow into a channel at each time point is equal to 1:

$$\sum_{k=1}^{K} \mathrm{ffADTF}_{ik}(t) = 1. \tag{11}$$

To investigate the features of the effective connectivity network during epileptic seizures, we calculated the ffADTF in the δ (1–4 Hz), θ (4–8 Hz), α (8–13 Hz), β (13–30 Hz), and γ (30–50 Hz) frequency bands in five representative 5-s seizure epochs (I: pre-seizure, II: early seizure, III: mid-seizure, IV: late seizure, and V: post-seizure) of all 14 seizures across all patients. The pre-seizure and early seizure epochs were selected 5 s before and after the seizure onset time (t_{SO}), respectively. The late seizure and post-seizure epochs were selected 5 s before and after the seizure termination time (t_{ST}), respectively. The t_{SO} and the t_{ST} were determined by the neurologists. The mid-seizure epoch was chosen from 2.5 s before and after the middle time point of the whole seizure period.

Graph theoretical analysis

Topological properties of the brain network were evaluated by the graph metrics at the small scale of single regions, i.e., graph metrics on single nodes. In the brain network, each electrical channel denotes a node. Each value in the weighted directed connectivity matrix ffADTF_{ij} represents the connection weights from node j to node i, i.e., the edge weight of the network. Transpose ffADTF_{ij} and use a_{ij} to indicate the weights from node i to node j. In directed networks, a_{ij} does not necessarily equal a_{ji}. K is the number of ECoG channels. Five graph metrics were used in the study: out-degree, closeness centrality, betweenness centrality, clustering coefficient, and local efficiency. All graph metrics were computed using the Brain Connectivity Toolbox (brain-connectivity-toolbox.net) [18].

To investigate the topological properties of the ffADTF effective connectivity network during different seizure periods, we calculated the graph metrics of five frequency bands in five seizure epochs of all seizures.

Out-degree

The out-degree OD_i quantified the information outflow of a node i:

$$OD_i = \sum_{j=1,j\neq i}^{K} a_{ij}. \quad (12)$$

Nodes with high OD values output more information to other nodes in a network.

Closeness centrality

The closeness centrality CC_i of a node i was defined as the reciprocal of the sum of the shortest path length between the node i with all other nodes [7]:

$$CC_i = \frac{K-1}{\sum_{j=1,j\neq i}^{K} d_{ij}}, \quad (13)$$

where d_{ij} is the directed shortest path length from node i to node j:

$$d_{ij} = \sum_{a_{ij}\in g_{i\to j}} f(a_{ij}). \quad (14)$$

In the weighted correlation network, higher correlations are interpreted as shorter distances. $f(a_{ij}) = \frac{1}{a_{ij}}$ is a mapping from weight matrix to length matrix and $g_{i\to j}$ is the shortest path from node i to node j.

Nodes with high values of CC communicate the information with the other nodes faster than the others.

Betweenness centrality

The betweenness centrality BC_i of a node i was defined as follows[7]:

$$BC_i = \frac{1}{(K-1)(K-2)} \sum_{h=1,h\neq j,h\neq i}^{K} \sum_{j=1,j\neq i}^{K} \frac{\rho_{hj}(i)}{\rho_{hj}}, \quad (15)$$

where ρ_{hj} is the number of directed shortest paths from node h to node j, and $\rho_{hj}(i)$ is the number of directed shortest paths from h to j that pass through i.

Nodes with high values of BC participate in a larger number of shortest paths and act as hubs in a network.

Clustering coefficient

The clustering coefficient C_i of a node i was defined as follows [6]:

$$C_i = \frac{t_i}{(OD_i + ID_i)(OD_i + ID_i - 1) - 2\sum_{j=1,j\neq i}^{K} a_{ij}a_{ji}}, \quad (16)$$

where t_i is the number of directed triangles around a node i:

$$t_i = \frac{1}{2} \sum_{h=1,h\neq j,h\neq i}^{K} \sum_{j=1,j\neq i}^{K} (a_{ij} + a_{ji})(a_{ih} + a_{hi})(a_{jh} + a_{hj}), \quad (17)$$

and ID_i is the in-degree of a node i:

$$ID_i = \sum_{j=1,j\neq i}^{K} a_{ji}. \quad (18)$$

The clustering coefficient quantifies the number of connections that exist between the nearest neighbours of a node as a proportion of the maximum number of possible connections [30]. Nodes with high values of C tend to cluster together with more nearest neighbours in a network.

Local efficiency

As an alternative to the clustering coefficient, the local efficiency LE_i of a node i was defined as follows [18]:

$$LE_i = \frac{1}{2} \frac{\sum_{h=1,h\neq j,j\neq i}^{K} \sum_{j=1,j\neq i}^{K} (a_{ij} + a_{ji})(a_{ih} + a_{hi}) \left(\frac{1}{d_{jh(N_i)}} + \frac{1}{d_{hj(N_i)}} \right)}{(OD_i + ID_i)(OD_i + ID_i - 1) - 2\sum_{j=1,j\neq i}^{K} a_{ij}a_{ji}}, \quad (19)$$

where $d_{jh}(N_i)$ is the length of the directed shortest path from node j to node h that contains only neighbours of i.

Statistical analysis

Since there is a highly nonlinear relation between the ADTF and the time series from which it is derived, the traditional parametric statistical methods cannot be applied [32]. Instead, random phases' surrogate data testing [15, 24], a nonparametric method, is used to assess the statistical significance of the ffADTF. The null hypothesis was proposed, stating that there exists no causal relationship among different channels of the ECoG signals. Phases and amplitudes of the ECoG data were first obtained by Fourier transform. We randomly shuffled the phases and used the new phases and the original amplitudes to generate the surrogate ECoG data using inverse Fourier transform. This phase shuffling process destroys the causality among ECoG signals, while

preserving the spectral structure of the ECoG data, which is critical, since the ffADTF is a frequency-dependent measure. Then, the surrogate ECoG data were used to calculate the surrogate ffADTF. We implemented this procedure 100 times. If 95% of the time, the original ffADTF was greater than the surrogate ffADTF, we rejected the null hypothesis, and the ffADTF was considered statistically significant.

Kruskal–Wallis test (*kruskalwallis.m*) and multiple comparison test (*multcompare.m*) in the Matlab Statistics Toolbox were used to assess the significant difference of the graph metrics among different cortical regions in the transient seizure onset network. The graph metric values were presented using the boxplot. $p < 0.05$, $p < 0.01$, $p < 0.001$ were considered significant difference and marked with the notation *, **, and ***, respectively.

An illustration of the main steps of the effective connectivity and graph theoretical analyses of the epileptic brain is presented in Fig. 1.

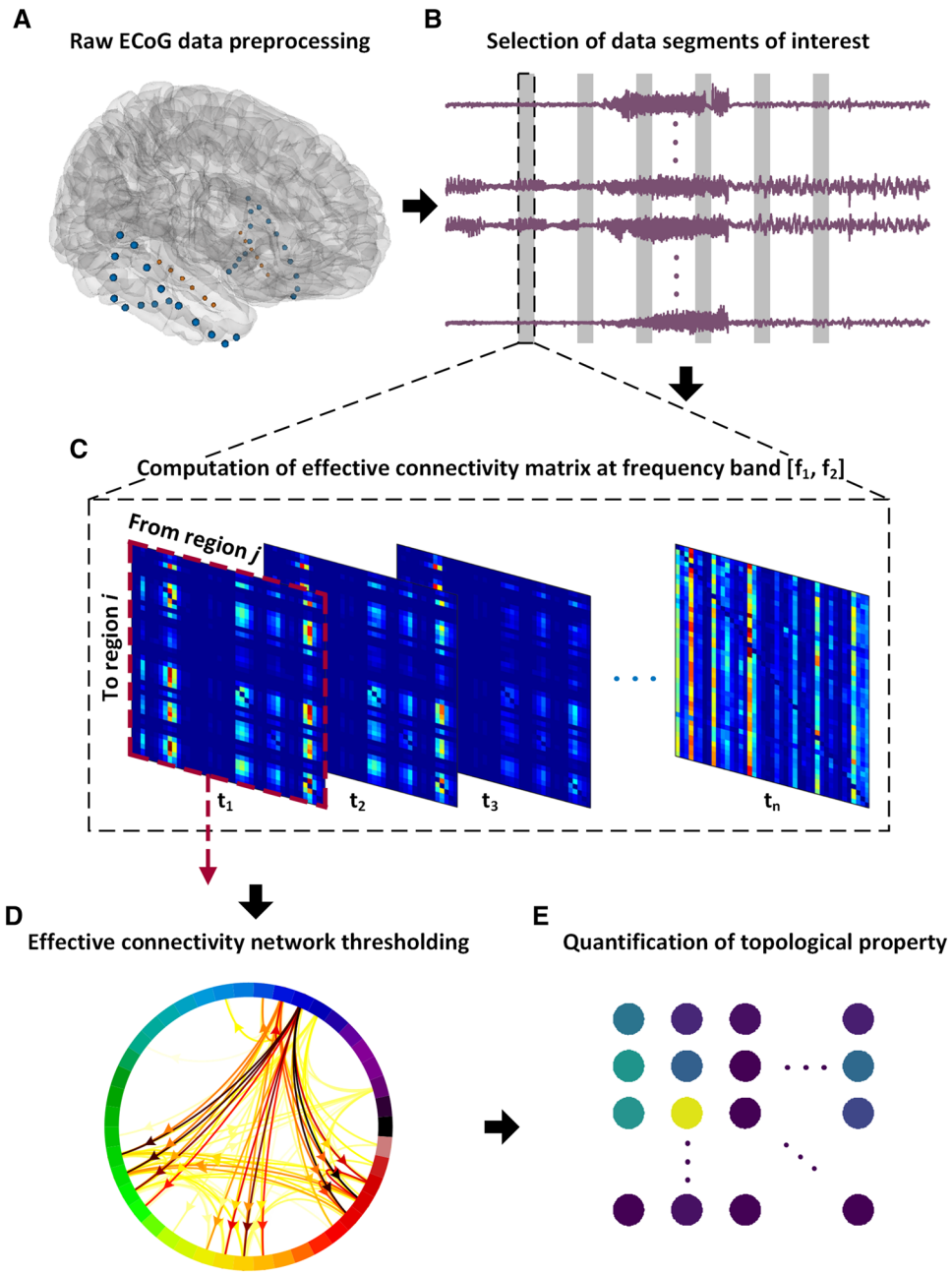

Fig. 1 Illustration of the main steps of the effective connectivity and graph theoretical analyses. **a** Preprocessing of the raw ECoG data: down-sampling to 256 Hz and 0.2-Hz high-pass filter, standardized z-scores, and removal of power frequency noise (50 Hz), harmonic noises, large-amplitude artifacts, and bad channels. **b** Select the data segments of interest: five representative 5-s data epochs, i.e., pre-seizure, early seizure, mid-seizure, late seizure, and post-seizure. **c** Calculate the directed and weighted effective connectivity matrix in the frequency band $[f_1, f_2]$: the ffADTF was calculated in the δ (1–4 Hz), θ (4–8 Hz), α (8–13 Hz), β (13–30 Hz), and γ (30–50 Hz) frequency bands of each epoch. **d** Effective connectivity thresholding: the top 5% of the strong connections were displayed in the ffADTF connectivity networks. **e** Quantify the topological properties using graph metrics (out-degree, closeness centrality, betweenness centrality, clustering coefficient, and local efficiency): the graph metrics were calculated at the small scale of single nodes and the total graph metrics in each cortical region were evaluated and compared with the clinical SOZ and resected regions

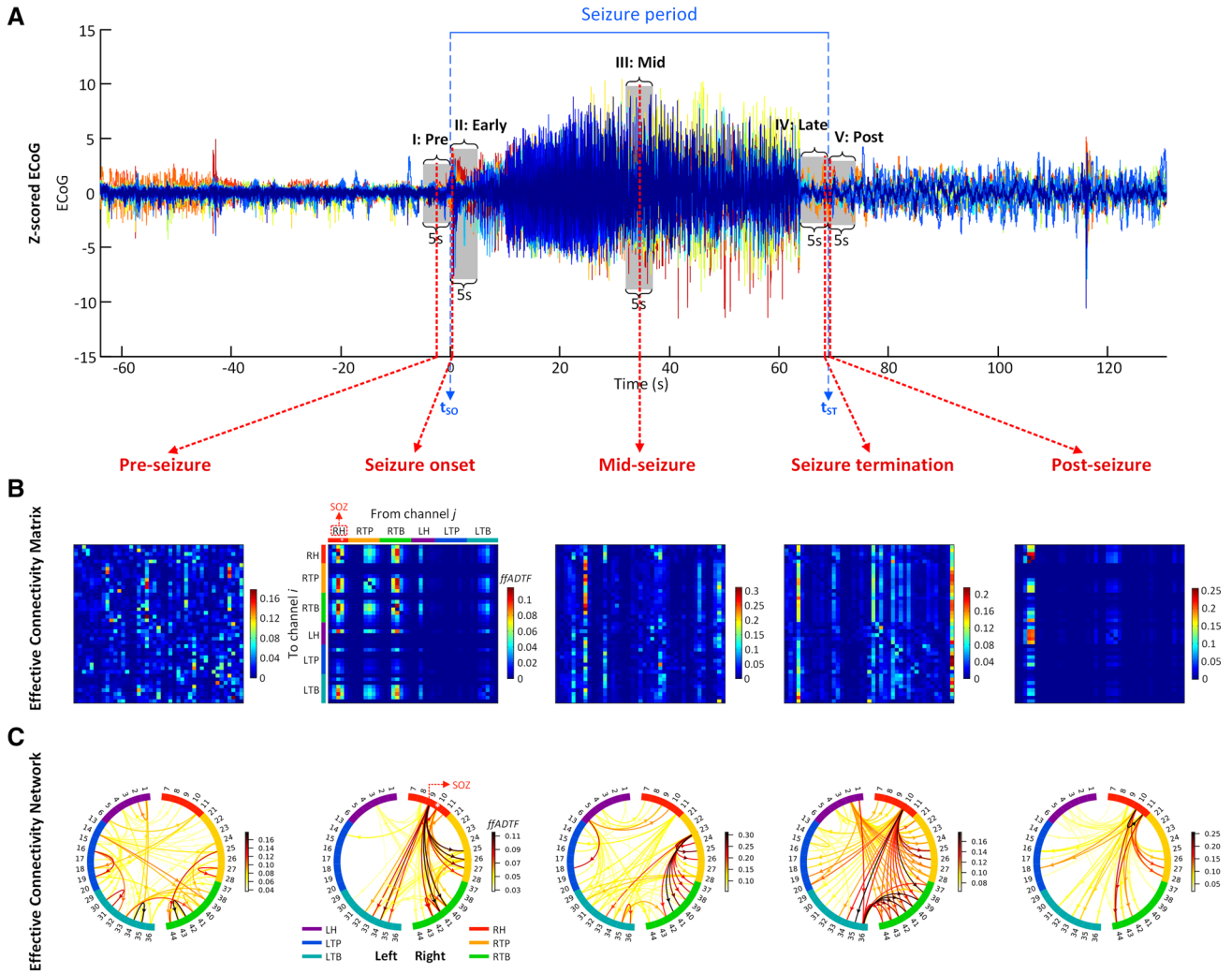

Fig. 2 Effective connectivity analysis results of the θ frequency band in seizure #1 of patient A. **a** Z-scored ECoG data of 43 channels in patient A, including a complete epileptic seizure, which is indicated by two blue dashed lines delineating the seizure onset time t_{SO} to the seizure termination time t_{ST}. Five representative 5-s seizure epochs were selected for the effective connectivity analysis (I: pre-seizure, II: early seizure, III: mid-seizure, IV: late seizure, and V: post-seizure), which are marked with light grey rectangles. In addition, five representative time points (pre-seizure, seizure onset, mid-seizure, seizure termination, and post-seizure) in these epochs were chosen to present the effective connectivity results in different time periods of temporal lobe epileptic seizures. **b** The ffADTF effective connectivity matrix from channel j to channel i. Channels with the same colour belong to the same electrode trip (red: right hippocampus, yellow: right temporal pole, green: right temporal base, purple: left hippocampus, blue: left temporal pole, and cyan: left temporal base). The right hippocampus and the channel marked with a white asterisk are the SOZ and SOC identified by clinical neurologists, respectively. The ffADTF effective connectivity network at five representative time points of an epileptic seizure

Results

Dynamic effective connectivity networks during epileptic seizures

The z-scored ECoG data of all channels for a representative patient (patient A, seizure #1), containing a complete epileptic seizure, and the data of pre- and post- seizures are shown in Fig. 2a. The seizure period is indicated by two blue dashed lines delineating the t_{SO} to the t_{ST}. Five seizure epochs were marked with light grey rectangles. Due to the time-variant ffADTF of each sample point, the ffADTF effective connectivity matrices and corresponding effective connectivity networks in the θ frequency band of five representative time points of each epoch are selected and shown in Fig. 2b, c. The top 5% of strong connections were presented in the effective connectivity network. Depth electrodes were implanted in the left hippocampus (LH) and right hippocampus (RH) in this patient. Cortical electrode strips were placed on the left temporal pole (LTP), left temporal base (LTB), right temporal pole (RTP), and right temporal base (RTB). The SOZ, i.e., RH and the seizure onset

channel (SOC), i.e., channel 10 (white asterisk) determined by clinical epileptologists are marked in the figure.

Because of the high temporal resolution, the ffADTF is able to characterize the dynamic epileptic connectivity network during the whole seizure. The asymmetrical effective connectivity ffADTF matrix was weighted and directed, thus quantifying the connection strength and detecting the connection direction. The effective connectivity matrices and its corresponding networks varied during the different seizure periods. Before the seizure onset time, a uniform network was presented during all seizures. As shown in Fig. 2b, c, the effective connectivity among all channels was uniform, and there was no obvious source activity. Particularly, some strong connections from the SOCs occasionally emerged during this period in the low-frequency bands of seizure #3 (δ and θ) in patient A, seizure #4 (δ, θ and α) in patient B, and seizure #10 (θ and α) and seizure #11 (δ, θ and α) of patient F, and even from the side contralateral to the SOZ of seizure # 12 (θ and α) of patient G. At the seizure onset time, the strong epileptic sources were mainly derived from the regions where the SOZ was located and some other ipsilateral regions involved in epileptogenic activity in the δ, θ and α frequency bands in most seizures. In the effective connectivity results of seizure #1 in patient A, strong connections from the RH, RTP, and RTB to the other channels appeared in both the right and left hemispheres, particularly on the ipsilateral side (Fig. 2b, c). This effective connectivity network that emerged at the seizure onset time remained for approximately 43 ms. However, the strong epileptic sources were found not only on side ipsilateral to the SOZ but also on side contralateral to the SOZ in the seizure #5 (δ) in patient C, seizure #10 (δ) and seizure #11 (δ, θ, and α) of patient F, seizure #12 (δ, θ, α, and β), seizure #13 (δ, θ, α, and β) and seizure #14 (δ, θ, α, and β) of patient G when the seizures began. The durations of the transient seizure onset network in all seizures are illustrated in Table 2. The seizure-specific durations ranged from 19 to 54 ms, with a mean value of 42 ms. Compared with the clinical epilepsy surgery results, the channels with strong connections in the transient seizure onset ffADTF network were included in the resection regions identified by the epileptologists in the Engel Class I (patients A, D, and E) and Engel Class II (patient B) patients, and they were also located in some other regions on the ipsilateral or contralateral side of the resection regions in the Engel Class II (patient C) and Engel Class III (patient F and G) patients. Then, the epileptic network changed to networks with irregular features. Strong epileptic sources were generated from the side ipsilateral or contralateral to the SOZ or from both sides of the cortex. The networks of the two time points in the mid-seizure and late seizure epochs of seizure #1 in patient A were selected as the examples of the time-varying effective connectivity networks, where the strong connections originated only from the RTP in the mid-seizure epoch and from both the RH and the contralateral LTB as the seizure approached its termination. Interestingly, at the post-seizure time, just after the seizure termination, clear, strong connections from the SOZ RH to other areas were established again, remaining for approximately 300 ms and converting to an irregular connectivity network afterwards. However, this special post-seizure network only appeared in the δ and θ frequency bands of seizure #1 in patient A and seizure #8 in patient E (the average duration of the post-seizure networks was 400 ms) rather than in all patients.

High values of graph metrics in the transient seizure onset network localize the seizure onset zone and epileptogenic zones

The distributions of the graph metrics across all channels in the θ frequency band at the five seizure time points presented in Fig. 2a are shown in Fig. 3. Typically, neurosurgeons avoid functional brain areas and resect the tissue slightly outside the defined EZ to minimize the risk of a secondary surgery. It can be seen in Fig. 3 that the distribution of the graph metrics differed across the seizure epochs. In the pre-seizure epoch, the high values of OD, CC, C, and LE appeared in both the left and right hemispheres, i.e., the distribution was relatively uniform. However, only a few channels with high BC were found on both sides. Conversely, almost all the high values of graph metrics were on the right side at seizure onset time. In addition, the highest OD and CC (marked with max on the channel) at the seizure onset time appeared in the RH, which was the SOZ determined by clinical epileptologists. The highest BC, C, and LE appeared in the RTB which was included in the clinical resection areas. Subsequently, all the highest graph metrics were in the RTP at the selected time of the mid-seizure period. As the seizure reached its termination, high values of graph metrics were located in both the RH and the contralateral side. After the seizure termination, high values of OD, BC, C, and LE were found only in a few channels in the RH, while a high value of CC appeared on many channels in both hemispheres.

Moreover, due to the emergence of the transient seizure onset network and its high relevance to the SOZ and the EZ, we generated a hypothesis, stating that the graph metrics in the SOZ and the EZ were higher than that in the other areas in the transient seizure onset network. We first calculated the total graph metric, i.e., the sum of the graph metric at all time points, of each channel in the seizure-specific transient seizure onset network in each frequency band of all seizures. The total OD, CC, BC, C, and LE of the 43-ms seizure onset network in an Engel Class I patient (seizure #1, θ frequency band) are shown in Fig. 4, depicted using bars. As shown in Fig. 4, high values of graph metrics appeared mainly in the right temporal lobe, especially in the RH and

Table 2 Seizure-specific results of cortical area with highest mean of graph metrics in the transient seizure onset network

Engel Class		I	I	I	I	I	I	I	II	II	III	III	III	III	III
Seizure/patient		#1/A	#2/A	#3/A	#6/D	#7/D	#8/E	#9/E	#4/B	#5/C	#10/F	#11/F	#12/G	#13/G	#14/G
Duration (ms)		43	40	40	51	19	43	40	54	39	51	27	52	43	41
OD	δ	**RH**	**RH**	LTB	**LH**	**LH**	**RTB**	RFPL	**LTB**	**LH**	**RTP**	RTO	LTP	LTO	**RTB**
	θ	**RH**	**RH**	LTB	**LH**	**LH**	**RTB**	RFPL	**LTB**	**LH**	**RTP**	RTO	LTP	LTO	**RTB**
	α	**RH**	**RH**	LTB	**LH**	**LH**	**RTB**	RFPL	**LTB**	**LH**	**RTP**	RTO	LTP	LTO	**RTB**
	β	**RH**	**RH**	LTB	**LH**	**LH**	RPTL	RPTL	**LTB**	**LH**	**RTP**	RTO	LTP	LTO	**RTB**
	γ	**RH**	**RH**	LTB	**LH**	**LH**	RPTL	RPTL	**LTB**	LTPB	**RTB**	RTO	**RTB**	LTO	RTO
CC	δ	**RH**	**RH**	LTB	**LH**	**LTB**	**RTB**	RFPL	**LTB**	**LH**	**RTP**	RTO	LTP	LTO	**RTB**
	θ	**RH**	LH	LTB	**LH**	RTB	**RTB**	RFPL	**LTB**	**LH**	**RTP**	RTO	LTP	RTO	**RTB**
	α	**RH**	LH	LH	**LH**	RTB	RPTL	RFPL	**LTB**	RH	**RTP**	RTO	LTP	RTO	**RTB**
	β	**RH**	LH	LH	**LH**	RTB	RPTL	RPTL	**LTB**	RH	**RTB**	RTO	LTP	RTO	**RTB**
	γ	**RH**	**RH**	LH	**LH**	RTB	RPTL	RFPL	**LTB**	LTPB	**RTB**	RTO	RTO	RTO	RTO
BC	δ	**RH**	**RH**	LTB	**LH**	**LH**	RPTL	RFPL	**LTB**	**LH**	**RTP**	RTO	LTP	LTO	RTO
	θ	**RH**	**RH**	LTB	**LH**	**LH**	RPTL	RFPL	**LTB**	**LH**	**RTP**	RTO	LTP	LTO	RTO
	α	**RTB**	**RH**	LTB	**LH**	RH	RPTL	RFPL	**LTB**	**LH**	**RTP**	RTO	LTP	LTO	RTO
	β	**RTB**	**RH**	LTB	**LH**	**LH**	RPTL	RFPL	**LTB**	**LH**	**RTP**	RTO	LTP	LTO	RTO
	γ	**RTB**	**RH**	LTB	**LH**	**LH**	RPTL	RFPL	**LTB**	LTPB	LTO	RTO	LTP	LTO	RTO
C	δ	**RH**	**RH**	LTB	**LH**	RTB	**RTB**	RFPL	**LTB**	**LH**	**RTP**	RTO	LTP	LTO	**RTB**
	θ	**RH**	**RH**	LTB	**LH**	RTB	**RTB**	RFPL	**LTB**	**LH**	**RTP**	RTO	LTP	LTO	**RTB**
	α	**RH**	**RH**	LTB	**LH**	RTB	**RTB**	RFPL	**LTB**	RH	LTO	RTO	LTP	LTO	**RTB**
	β	**RH**	**RH**	LTB	**LH**	**LH**	**RTB**	RFPL	**LTB**	**LH**	LTO	RTO	LTP	LTO	**RTB**
	γ	**RH**	**RH**	LTB	**LH**	**LH**	RPTL	RFPL	**LTB**	**LH**	LTO	RTO	**RTB**	**RTB**	RTO
LE	δ	**RH**	**RH**	LTB	**LH**	RTB	**RTB**	RFPL	**LTB**	**LH**	**RTP**	RTO	LTP	LTO	**RTB**
	θ	**RH**	**RH**	LTB	**LH**	RTB	**RTB**	RFPL	**LTB**	**LH**	**RTP**	RTO	LTP	LTO	**RTB**
	α	**RH**	**RH**	LTB	**LH**	RTB	**RTB**	RFPL	**LTB**	RH	LTO	RTO	LTP	LTO	**RTB**
	β	**RH**	**RH**	LTB	**LH**	RH	RPTL	RFPL	**LTB**	**LH**	LTO	RTO	LTP	LTO	**RTB**
	γ	**RH**	**RH**	LTB	**LH**	**LH**	RPTL	RFPL	**LTB**	LTPB	LTO	RTO	**RTB**	**RTB**	RTO

The same cortical region as the clinically identified SOZ is indicated in bold font and with a border. The cortical region that belongs to the clinical resected regions is only indicated in bold

L left, *R* right, *H* hippocampus, *TL* temporal lobe, *TP* temporal pole, *TB* temporal base, *PTL* posterior temporal lobe, *PTB* posterior temporal base, *FPL* frontal–parietal lobe, *TO* temporal–occipital, *OD* out-degree, *CC* closeness centrality, *BC* betweenness centrality, *C* clustering coefficient, *LE* local efficiency

RTB. In Fig. 4a, b, d, e, the highest OD, CC, C, and LE were generated by channel 9 which was located in the RH and was the neighbouring contact of the clinically identified SOC (marked with a white asterisk). In Fig. 4c, the highest BC appeared in channel 41, which was located in the RTB and included in the clinical resection areas. Moreover, the BC of most channels were found to be equal to zero, which means that these channels participate in none of the shortest paths in the transient seizure network. Channel 9 in the RH and channel 41 in the RTB acted as the essential hubs in the network and removal of areas where these two channels were located will have the most significant effect on the seizure onset network performance.

Then, the graph metrics of the seizure-specific transient seizure onset network in each frequency band of all seizures in each electrode strip, i.e., each involved cortical region, are described by boxplots. Figure 5 presents the boxplots of OD, CC, BC, C, and LE of the transient seizure onset network (Engel Class I patient A, seizure #1, θ frequency band). The OD, BC, CC, and LE in the RH were significantly higher than the graph metric values in the other two regions on the ipsilateral side (RTP and RTB) and in

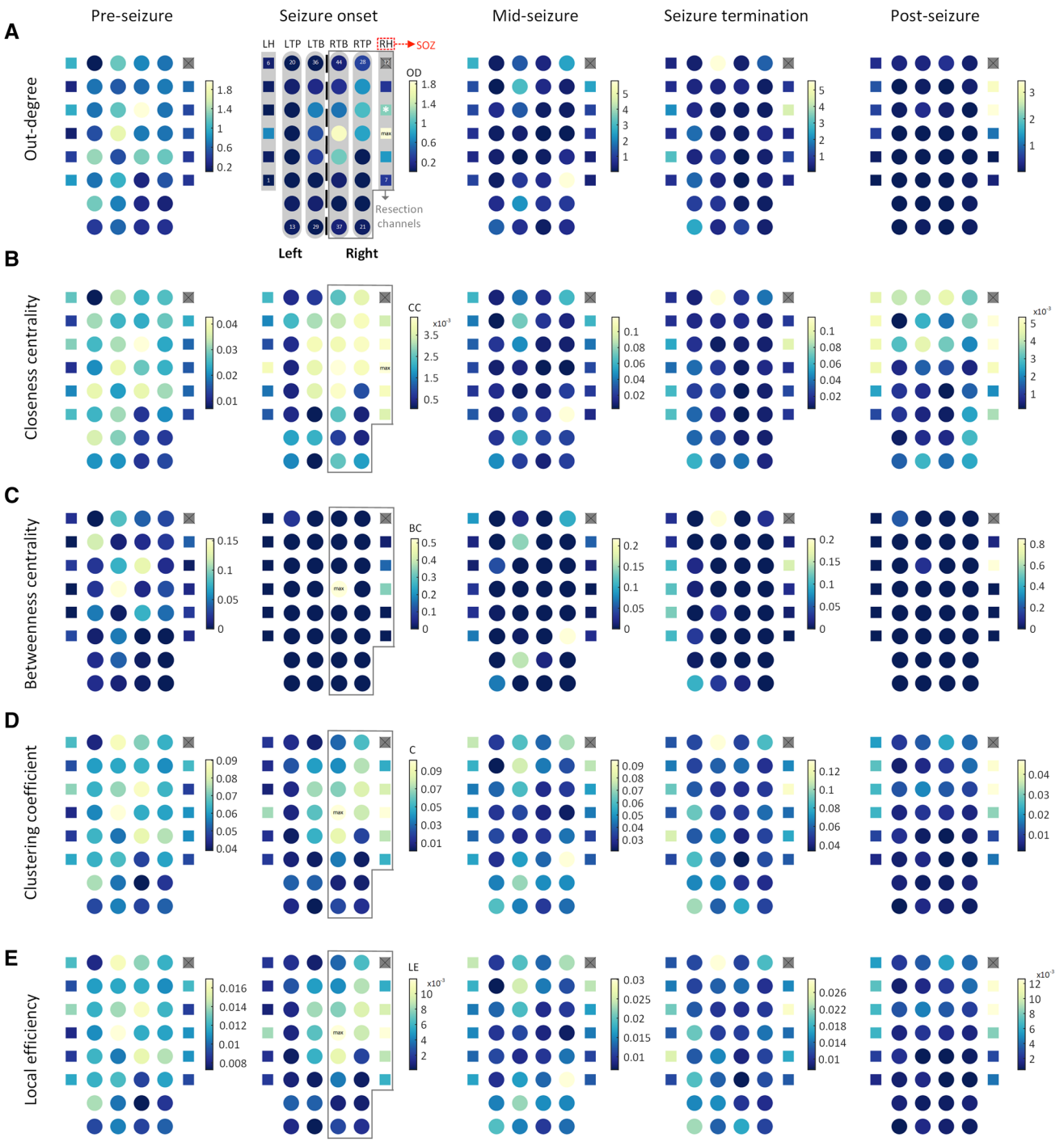

Fig. 3 Distribution of the graph metrics across all channels at five representative seizure time points is presented in Fig. 2. Depth electrodes (RH and LH) and cortical electrode strips (RTP, RTB, LTP, and LTB) are denoted by squares and circles, respectively. Channels in the grey rectangle were included in the resection areas in the clinical surgery. Channel 12 was the bad channel, as assessed by visual inspection. Channel 10 with a white asterisk was the SOC determined by clinical epileptologists

all regions on the contralateral side (LH, LTP, and LTB) (Kruskal–Wallis test). The CC in the RH was significantly higher than that in RTB and all regions on the contralateral side (Kruskal–Wallis test). These results demonstrated that the RH region, the SOZ identified by clinical epileptologists, communicated the most information to the other regions at the fastest speed, clustered together with the most numbers of nearest neighbours and acted as the most essential hub in the transient seizure onset network. Moreover, the OD, CC, C, and LE in RTB and RTP regions were significantly

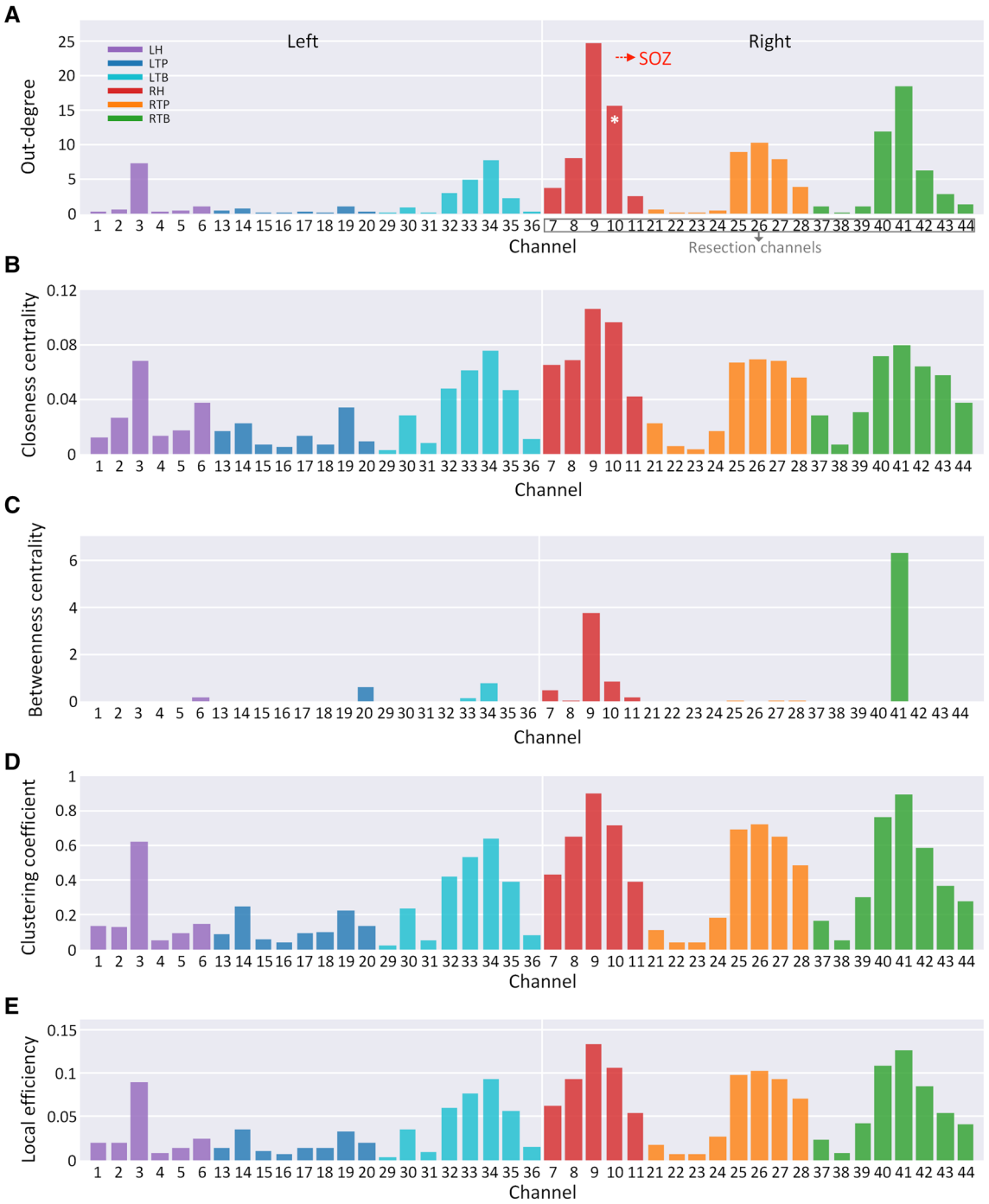

Fig. 4 Total graph metrics of each channel in the transient seizure onset network of the θ frequency band in seizure #1 of patient A

higher than the values in some regions on the contralateral hemisphere, which means that RTB and RTP regions also worked as the important cortical areas in the transient seizure onset network.

The cortical regions with highest means of graph metrics in the seizure-specific transient seizure onset network in each frequency band of all seizures are presented in Table 2. The same cortical region as the clinically identified SOZ is indicated in bold font and with a border. The cortical region that belongs to the clinical resected regions is only indicated in bold.

In terms of the Engel Class I, patient A, the highest means were found in RH in almost all frequency bands and graph metrics of seizure #1 and #2, while they were found in the

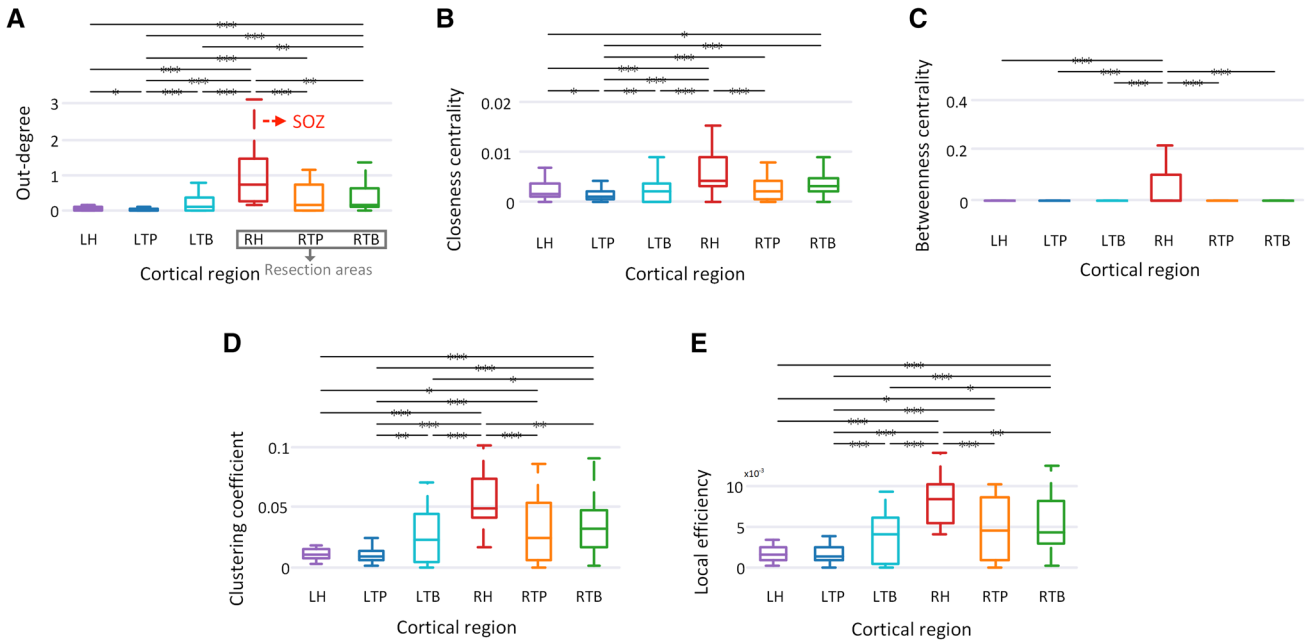

Fig. 5 Boxplot of the graph metrics in each cortical area in the transient seizure onset network of the θ frequency band in seizure #1 of patient A

contralateral side LTB and LH of seizure #3. The durations of the transient seizure onset networks of these three seizures were almost the same. Another Engel Class I, patient D, the locations with the highest means were the LH in all frequency bands and graph metrics of seizure #6, which were consistent with the clinical identified SOZ. However, in seizure #7, the same locations appeared in almost all the frequency bands in OD and BC, while in none frequency bands in CC and only in high-frequency bands (β and γ) in C and LE. The duration of the transient seizure onset network of these two seizures exhibited a substantial difference, i.e., the duration of seizure #6 (51 ms) was more than 2.5 times than that of seizure #7 (19 ms), which was unique for patient A. Unlike the patients A and D, the Engel Class I patient E had no same highest mean values of graph metric as the clinical identified SOZ. Only in the seizure #8, the low-frequency bands δ, θ, and α of OD, CC, C, and LE, the area RTB with the highest mean belonged to the clinical resected regions. Regarding the Engel Class II, patient B, the locations with the highest means were the LTB in all frequency bands and graph metrics, which was the neighbouring cortical area of the SOZ, i.e., LTP that with the second highest means. Another Engel Class II patient C, the LH that is the same as the clinical identified SOZ, was the highest mean in δ and θ frequency bands of all graph metrics and in higher frequency bands of OD, BC, C, and LE. In the case of Engel Class III, patient F, the highest means were found in the δ, θ, α, and β frequency bands of OD and BC, in the δ, θ, and α frequency bands of CC, and δ, θ frequency bands of C and LE in seizure #10. In seizure #11, the cortical area with the highest means was the RTO in all the frequency bands and graph metrics, which was neither consistent with the SOZ nor included in the resected regions. The duration of seizure #10 (51 ms) was twice that of seizure #11 (27 ms). In Engel

Table 3 Proportion of the same cortical area with highest mean of graph metrics as the clinical identified SOZ

Graph metric	Engel class			Frequency band				
	I (%)	II (%)	III (%)	δ (%)	θ (%)	α (%)	β (%)	γ (%)
OD	57	40	16	43	43	43	43	29
CC	34	20	12	36	29	21	14	21
BC	46	40	16	43	43	29	36	21
C	49	40	8	36	36	21	36	36
LE	46	30	8	36	36	21	29	29
Mean	46.4	34.0	12.0	38.8	37.4	27.0	31.6	27.2

OD out-degree, *CC* closeness centrality, *BC* betweenness centrality, *C* clustering coefficient, *LE* local efficiency

Class III patient G, no results were the same as the clinical identified SOZ. Only RTB in γ frequency band of OD, C, and LE in seizure #12, RTB in γ frequency band of C and LE in seizure #13, RTB in δ, θ, α, and β frequency bands of OD, CC, C, and LE in seizure #14, were belong to the resected regions. The durations of these three seizures were more than 40 ms.

The proportions of the same cortical regions with the highest mean of graph metrics as the clinical identified SOZ of each graph metric in three different Engel Classes and in five different frequency bands are illustrated in Table 3. In terms of different Engel Classes, the proportion of Engel Class I was greater than the proportion of Engel Class II and the proportion of Engel Class II was greater than the proportion of Engel Class III in all the graph metrics. The mean proportions of Engel Class I, II, and III were 46.4%, 34% ,and 12%, respectively. It was also found that the OD was the largest in all Engel Classes compared with the other four graph metrics. In Engel Class I patients, the proportion rank was OD > C > BC = LE > CC, which means that the out-degree and clustering coefficient are more likely to localize the cortical areas that are the same as the clinical identified SOZ. Regarding different frequency bands, the mean proportions of δ and θ frequency bands were larger than the proportions of the higher frequency bands. The OD had the same proportion (43%) in δ, θ, α, and β frequency bands, and the BC had the same proportion (43%) in δ and θ frequency bands, which was the largest value among the five graph metrics. The proportion of CC in δ band was larger than that in the other four higher frequency bands. C had the same proportions in δ, θ, β, and γ frequency bands (36%), which was larger than that in the α frequency bands. LE had the same values in the δ and θ frequency bands (36%) as well as in the β and γ frequency bands (29%), which were larger than the values in α frequency bands.

Discussion

This study investigated the time-varying characteristics of effective connectivity in the epileptic brain networks in 14 seizures of seven patients with TLE, using the measure of the ffADTF combined with five graph metrics. The effective connectivity was evaluated and compared across five frequency bands and five representative seizure periods. The locations of the strong epileptic sources found by using these measures were compared with the SOZ and EZ identified by epileptologists, as well as with the results of epilepsy surgery.

The main difference between DTF and ADTF is the 'adaptive' which can be explained as 'time-variant'. Given a data epoch, we can get only one connectivity matrix DTF using the multivariate autoregressive (MVAR) model. However, the connectivity matrices ADTF at each sample point can be obtained using the AMVAR model which is also called a TVAR model. The ADTF-based measure ffADTF can detect the dynamic change of the effective connectivity, with a high temporal resolution at specific frequency bands. This allows us to gain useful information in terms of dynamic causality from the non-stationary signals in the epileptic brain.

From the effective connectivity network results, the ffADTF connectivity networks were time-dependent throughout the entire period of the seizure. Before the seizure onset, uniform networks were observed most of the time across all five frequency bands of all patients, with some strong connections occasionally appearing in the low-frequency bands (δ, θ, α) from the SOC of two Engel Class I and II patients and from side contralateral to the SOZ of one Engel Class III patient. These results illustrated that some strong low-frequency epileptogenic activity may emerge before a seizure, but they do not trigger seizures. The location of this strong activity is just within the region of the SOZ, as identified by epileptologists, or the region that is not identified as the EZ. These findings lead us to suspect that the location of strong information communication before a seizure might be the potential SOZ or EZ.

At the seizure onset time, strong connections were observed between the regions where the SOZ was located and some ipsilateral EZ mainly on the side where the SOZ was located in all Engel Class I patients and one Engel Class II patient. However, strong epileptic activity was generated on both the ipsilateral and contralateral sides of the SOZ in one Engel Class II patient and all Engel Class III patients. In regard to the Engel II and III patients, there still existed varying degrees of seizures after their first resection surgeries, meaning that there were some regions with abnormal epileptic discharge in the cerebral cortex that were not resected. These regions are likely to be the regions where the strong activity is generated outside the surgical resection areas in the ffADTF effectivity connectivity network. Therefore, the seizure onset network based on the ffADTF may detect potential EZ other than the ones identified by the epileptologists. Furthermore, the locations that the strong connections were generated from in the seizure onset network in the low-frequency δ, θ, and α bands were found to be more closely correlated with the SOZ and the EZ than those in the β and γ bands. However, high-frequency β and γ band activities demonstrated significantly more overlap with the SOZ than the low-frequency θ and α band activities in Wilke's studies [34, 35], which was inconsistent with our findings. This finding may have been due to the different seizure types and the large individual differences among the epileptic patients. Another important finding was that the seizure onset network that emerged at seizure onset time remained

for approximately 20–50 ms with strong connections generated from both the SOZ and other EZ, rather than rapidly changing to the other network patterns. This newly discovered transient seizure onset network is an important biomarker during the seizure period and could be a promising tool for the localization of the SOZ and the EZ.

In subsequent epileptic networks, the effectivity connectivity presented irregular features, which indicated that the strong epileptic activity was not only restricted in the ipsilateral hemisphere of the SOZ but was also propagated to the hemisphere contralateral to the SOZ. Finally, a special phenomenon was observed in the low-frequency δ and θ bands in two seizures of two Engel Class I patients at the seizure termination time. Strong connections from the SOZ to other areas were established again in a similar to that of the transient seizure onset network. A possible interpretation could be that the neurons in the SOZ in these two patients may, sometimes, serve as main controllers in both seizure onset and seizure termination.

In terms of the results of the distribution of graph metrics, high values of graph metrics corresponded to the channels that generated the strong connections in the effective connectivity networks. The information communication strength of each channel could be seen more intuitively, such that we are able to estimate which channels were the epileptogenic sources and played important roles in the epileptic network. In addition, in the transient seizure onset network as discussed above, the channels with high values of total graph metrics were located in the clinically identified SOZ and ipsilateral EZ in most Engel Class I and II patients and even in some contralateral areas in a few Engel Class II or III patients. In addition, the values of graph metrics of SOZ were found to be the largest among the cortical areas and the values of all EZs were significantly larger than other cortical areas in seizure-free patients. The SOZ is the area of the cortex from which abnormal rhythm of seizures are actually generated, and EZ is the area of the cortex that is indispensable for the generation of epileptic seizures [17]. In the process of the origination and propagation of epileptic information, SOZ and EZ involve more information generation and transfer than other cortical areas in the epileptic brain network. Different graph metrics evaluate the characteristics of the cortical areas in the epileptic brain from different aspects. The OD quantifies how much information is output, CC measures how long it will take to spread information, BC indicates how important the node is in the information transfer path, C and LE describe how much the node is clustered with other neighbours, which make it possible to detect the SOZ and EZ in the epileptic brain. In particular, the BC could locate the most important channels which acted as the essential hubs in the seizure onset network. These results illustrate that high values of graph metrics in the transient seizure onset network could provide a more accurate localization of the SOZ and the EZ for epileptologists in the preoperative assessment.

Furthermore, with regard to the seizure-specific results of cortical area with highest mean of graph metrics in the transient seizure onset network across the five frequency bands, more cortical areas with the highest mean of graph metrics were the same as the clinically determined SOZ existed in the low-frequency δ and θ bands and in Engel Class I patients than in higher frequency α, β, and γ bands and in Engel Class II and III patients. This result demonstrates that the SOZs in the Engel Class I patients are relatively centralized. Conversely, the SOZs in Engel Class II and III patients are relatively scattered. Some SOZs and EZs that were not resected in the first surgeries still exist; that is why, these patients have varying degrees of seizures after the resection surgeries. On the other hand, out-degree and clustering coefficient are more likely to localize the SOZ and EZ than closeness centrality, betweenness centrality, and local efficiency, illustrating that SOZ and EZ have a higher correlation with the amount of information output and the degree of clustering with the surrounding cortex in the seizure onset network. Moreover, the different durations of the transient seizure onset networks were probably due to the large individual differences among the patients and the different physiological statuses within the same patient.

However, our study had some limitations. Only 14 recorded seizures in seven patients were included. The same numbers of seizure in each Engel Class would be better to make a comparison. More patients with different Engel Classes will be included in our future work to further verify the findings. Depth electrodes and cortical electrode strips cannot completely ensure coverage of the entire SOZ and EZ. If some EZ located outside the regions are covered by the electrode strips, some locations of EZ would be omitted in both clinical visual analysis and effective connectivity analysis. In addition, invasive electrode strips or grids cannot be implanted in healthy individuals, so it is not possible to compare the differences in effective connectivity networks between epileptic patients and healthy subjects. High-density EEG recordings could be applied to effective connectivity analyses in future studies, which could provide more information on the connectivity features of the whole brain and obtain contrastive connectivity networks from a healthy control group. Other effective connectivity measures, such as the integrated ADTF [26, 27], masked ADTF [26], and spectrum-weighted ADTF [25], and measures of adaptive partial directed coherence [2, 28] can be used and compared. Although accurate localization of EZ using the ffADTF and graph metrics may lead to small resection regions, this still needs to be further verified in clinical preoperative evaluation and postoperative follow-up results in a large group of epileptic patients before this brain connectivity method can be applied in clinical practice.

In conclusion, the ffADTF combined with OD, CC, BC, C, and LE were used to investigate the time-varying effective connectivity of ECoG signals at a high temporal resolution in patients with temporal lobe epilepsy, which was evaluated and compared across different frequency bands and different seizure periods. Generation and propagation of strong epileptic activities can be observed from the ffADTF effective connectivity networks, and the location of the SOZ and EZ can be found using the high values of graph metrics in the newfound transient seizure onset effective connectivity network. Different graph metrics reflect the different characteristics of epileptic information communication among the cortical areas. Overall, our study proved that the high temporal resolution effective connectivity measure ffADTF combined with different graph metrics is able to provide a more precise localization of the SOZ and EZ, contributing to clinical preoperative assessments and reducing both the number of postoperative seizures and the probability of secondary surgeries.

Acknowledgements This research is supported by the Ph.D. grant of the Faculty of Information Technology in the University of Jyväskylä, Beijing Science & Technology Commission in Tongzhou District no. KJ2015CX004 and Beijing Municipal Science & Technology Commission no. Z161100002616001.

Compliance with ethical standards

Conflicts of interest On behalf of all authors, the corresponding author states that there is no conflict of interest.

Ethical approval This research has been approved by the Ethics Committees of Xuanwu Hospital, Capital Medical University and Luhe Hospital, Capital Medical University, and it has been performed in accordance with the ethical standards laid down in the 1964 Declaration of Helsinki and its later amendments.

References

1. Chiang S, Haneef Z (2014) Graph theory findings in the pathophysiology of temporal lobe epilepsy. Clin Neurophysiol 125:1295–1305
2. Coito A, Plomp G, Genetti M, Abela E, Wiest R, Seeck M, Michel CM, Vulliemoz S (2015) Dynamic directed interictal connectivity in left and right temporal lobe epilepsy. Epilepsia 56:207–217
3. Engel J Jr, Thompson PM, Stern JM, Staba RJ, Bragin A, Mody I (2013) Connectomics and epilepsy. Curr Opin Neurol 26:186–194
4. Engel J Jr (1993) Outcome with respect to epileptic seizures. In: Surgical treatment of the epilepsies, pp 609–621
5. Englot DJ, D'Haese PF, Konrad PE, Jacobs ML, Gore JC, Abou-Khalil BW, Morgan VL (2017) Functional connectivity disturbances of the ascending reticular activating system in temporal lobe epilepsy. J Neurol Neurosurg Psychiatry 88:925–932
6. Fagiolo G (2007) Clustering in complex directed networks. Phys Rev E Stat Nonlinear Soft Matter Phys 76:026107
7. Freeman LC (1978) Centrality in social networks conceptual clarification. Soc Netw 1:215–239
8. Friston K, Frith C, Frackowiak R (1993) Time-dependent changes in effective connectivity measured with PET. Hum Brain Mapp 1:69–79
9. Granger CW (1969) Investigating causal relations by econometric models and cross-spectral methods. Econometrica J Econ Soc 37:424–438
10. Haneef Z, Chiang S (2014) Clinical correlates of graph theory findings in temporal lobe epilepsy. Seizure 23:809–818
11. Kaminski MJ, Blinowska KJ (1991) A new method of the description of the information flow in the brain structures. Biol Cybern 65:203–210
12. Kramer MA, Cash SS (2012) Epilepsy as a disorder of cortical network organization. Neuroscientist 18:360–372
13. Kramer MA, Kolaczyk ED, Kirsch HE (2008) Emergent network topology at seizure onset in humans. Epilepsy Res 79:173–186
14. Neumaier A, Schneider T (2001) Estimation of parameters and eigenmodes of multivariate autoregressive models. ACM Trans Math Softw (TOMS) 27:27–57
15. Palus M, Hoyer D (1998) Detecting nonlinearity and phase synchronization with surrogate data. IEEE Eng Med Biol Mag 17:40–45
16. Ponten SC, Bartolomei F, Stam CJ (2007) Small-world networks and epilepsy: graph theoretical analysis of intracerebrally recorded mesial temporal lobe seizures. Clin Neurophysiol 118:918–927
17. Rosenow F, Luders H (2001) Presurgical evaluation of epilepsy. Brain 124:1683–1700
18. Rubinov M, Sporns O (2010) Complex network measures of brain connectivity: uses and interpretations. Neuroimage 52:1059–1069
19. Sakkalis V (2011) Review of advanced techniques for the estimation of brain connectivity measured with EEG/MEG. Comput Biol Med 41:1110–1117
20. Schlogl A, Roberts SJ, Pfurtscheller G (2000) A criterion for adaptive autoregressive models. In: Proceedings of the 22nd annual international conference of the IEEE engineering in medicine and biology society (Cat. No. 00CH37143). IEEE, pp 1581–1582
21. Schneider T, Neumaier A (2001) Algorithm 808: ARfit—a Matlab package for the estimation of parameters and eigenmodes of multivariate autoregressive models. ACM Trans Math Softw (TOMS) 27:58–65
22. Schwarz G (1978) Estimating the dimension of a model. Ann Stat 6:461–464
23. Storti SF, Galazzo IB, Khan S, Manganotti P, Menegaz G (2017) Exploring the epileptic brain network using time-variant effective connectivity and graph theory. IEEE J Biomed Health Inform 21:1411–1421
24. Theiler J, Eubank S, Longtin A, Galdrikian B, Farmer JD (1992) Testing for nonlinearity in time series: the method of surrogate data. Phys D 58:77–94
25. van Mierlo P, Carrette E, Hallez H, Raedt R, Meurs A, Vandenberghe S, Van Roost D, Boon P, Staelens S, Vonck K (2013) Ictal-onset localization through connectivity analysis of intracranial EEG signals in patients with refractory epilepsy. Epilepsia 54:1409–1418
26. van Mierlo P, Carrette E, Hallez H, Vonck K, Van Roost D, Boon P, Staelens S (2011) Accurate epileptogenic focus localization through time-variant functional connectivity analysis of intracranial electroencephalographic signals. Neuroimage 56:1122–1133
27. van Mierlo P, Coito A, Vulliémoz S, Lie O (2016) Seizure onset zone localization from many invasive EEG channels using directed functional connectivity. In: Signal Processing conference (EUSIPCO), 2016 24th european. IEEE, pp 255–259
28. Wang G, Sun Z, Tao R, Li K, Bao G, Yan X (2016) Epileptic seizure detection based on partial directed coherence analysis. IEEE J Biomed Health Inform 20:873–879
29. Wang J, Qiu S, Xu Y, Liu Z, Wen X, Hu X, Zhang R, Li M, Wang W, Huang R (2014) Graph theoretical analysis reveals disrupted

topological properties of whole brain functional networks in temporal lobe epilepsy. Clin Neurophysiol 125:1744–1756
30. Watts DJ, Strogatz SH (1998) Collective dynamics of 'small-world' networks. Nature 393:440–442
31. Wilke C, Ding L, He B (2007) An adaptive directed transfer function approach for detecting dynamic causal interactions. In: Engineering in medicine and biology society, 2007. EMBS 2007. 29th annual international conference of the IEEE. IEEE, pp 4949–4952
32. Wilke C, Ding L, He B (2008) Estimation of time-varying connectivity patterns through the use of an adaptive directed transfer function. IEEE Trans Biomed Eng 55:2557–2564
33. Wilke C, van Drongelen W, Kohrman M, He B (2010) Neocortical seizure foci localization by means of a directed transfer function method. Epilepsia 51:564–572
34. Wilke C, Worrell G, He B (2011) Graph analysis of epileptogenic networks in human partial epilepsy. Epilepsia 52:84–93
35. Wilke C, Worrell GA, He B (2009) Analysis of epileptogenic network properties during ictal activity. Conf Proc IEEE Eng Med Biol Soc 2009:2220–2223
36. Yaffe RB, Borger P, Megevand P, Groppe DM, Kramer MA, Chu CJ, Santaniello S, Meisel C, Mehta AD, Sarma SV (2015) Physiology of functional and effective networks in epilepsy. Clin Neurophysiol 126:227–236
37. Zhang H, Lai D, Xie C, Zhang H, Chen W (2016) Directed-transfer-function based analysis for epileptic prediction. In: Image and signal processing, biomedical engineering and informatics (CISP-BMEI), international congress. IEEE, pp 1487–1491
38. Zhang L, Liang Y, Li F, Sun H, Peng W, Du P, Si Y, Song L, Yu L, Xu P (2017) Time-varying networks of inter-ictal discharging reveal epileptogenic zone. Front Comput Neurosci 11:77

Affiliations

Ye Ren[1,2] · Fengyu Cong[2,3] · Tapani Ristaniemi[2] · Yuping Wang[4,5,6] · Xiaoli Li[7] · Ruihua Zhang[1]

1 Department of Geriatric Medicine, Beijing Luhe Hospital, Capital Medical University, No. 82, Xinhua South Street, Tongzhou District, Beijing 101149, China

2 Faculty of Information Technology, University of Jyväskylä, 40014 Jyvaskyla, Finland

3 School of Biomedical Engineering, Faculty of Electronic Information and Electrical Engineering, Dalian University of Technology, Dalian 116024, China

4 Department of Neurology, Xuanwu Hospital, Capital Medical University, Beijing 100053, China

5 Beijing Key Laboratory of Neuromodulation, Beijing 100053, China

6 Center of Epilepsy, Beijing Institute for Brain Disorders, Beijing 100053, China

7 State Key Laboratory of Cognitive Neuroscience and Learning, IDG/McGovern Institute for Brain Research, Beijing Normal University, No. 19 Xinjiekou Street, Haidian District, Beijing 100875, China